Functionalization of γ-Graphyne by Transition Metal Adatoms

Sunkyung Kim [a], Antonio Ruiz Puigdollers [b], Pablo Gamallo [b], Francesc Viñes [b,*], Jin Yong Lee [a,*]

[a] *Department of Chemistry, Sungkyunkwan University, Suwon 16419, Korea*
[b] *Departament de Ciència de Materials i Química Física & Institut de Química Teòrica i Computacional (IQTCUB), Universitat de Barcelona, c/Martí i Franquès 1, 08028 Barcelona, Spain*

Abstract

Transition Metal (*TM*) atom adsorption on γ-graphyne is here studied to unravel the electronic and magnetic properties tuning of this 2D carbon allotrope, with possible repercussions on molecular storage, sensing, and catalytic properties. A thorough density functional theory study, including dispersion, of the structural, energetic, diffusivity, magnetic, and doping properties for *all* 3*d*, 4*d*, and 5*d* TM adatoms adsorbed on γ-graphyne is provided. Overall, TMs strongly chemisorb on γ-graphyne acetylenic rings, except d^{10} group XII TMs which physisorb. Diffusion energy barriers span 0.5-3.5 eV and adatom height with respect the γ-graphyne sheet seems to be governed by TM atomic radius. All TMs are found to give *n*-doped γ-graphyne, where charge transfer decays along *d* series due to the increasing electronegativity of TMs. Middle TMs infer noticeable magnetism to γ-graphyne, yet magnetism is heavily quenched for early and late TMs. The large adsorption energies close to parent TM bulk cohesive energies, the high diffusion energy barriers, and the coulombic repulsion between positively charged TM adatoms provide a good environment for TMs to disperse over the graphyne.

* Corresponding authors: francesc.vines@ub.edu, jinylee@skku.edu

1. Introduction

In the latest years the carbon materials family of graphynes —two-dimensional carbon allotropes containing C atoms with *sp* and sp^2 hybridization states— have become a hub of research [1-3]. Despite they were theoretically hypothesized in 1968 [4], research on them was scarce for decades [5]. However, scientific endeavours on this class of materials have recently bloomed essentially driven from theoretical predictions. Density Functional Theory (*DFT*) predicted the existence of Dirac cones in α-, β-, and 6,6,12-graphynes, and a higher charge carrier conductivity compared to graphene [6,7], which was experimentally corroborated later on [8]. Such a high carrier mobility [9] can be used for practical materials; *e.g.* graphdiyne films have been used as a supporting material (or a substrate) to TiO_2 P25 photocatalysts in the course of methylene blue photodegradation [10,11], where the improved photocatalytic activity was explained by the higher charge transport and the better electronic coupling of graphdiyne with TiO_2. In spite of successful reports [12-15], further research needs to be spurred by theoretical simulations on their fruitful possible applications.

Aside from the aforementioned molecular electronics [8] and photocatalysis applications [10,11], graphynes have been suggested as suited materials for water desalination [16], a convenient matrix for Li-based batteries [17], and even good materials for the Oxygen Reduction Reaction (*ORR*) catalysis [18]. Similarly to graphene, graphynes properties can be modified and tuned by inserting certain heteroatoms such as N or B [19,20], or Ca decoration for H_2 storage purposes [21]. Certainly, most of the graphyne atomic literature dealt with alkali metal adsorption, in the context of alkali metal based batteries [17,22,23], or either alkali or alkali-earth metal adatoms as centres for H_2 storage [21,24,25].

Graphyne properties can be tuned by decoration with Transition Metal (*TM*) atoms. Note that graphene decorated by adsorption of TMs have been extensively studied (see Ref. [26] and references therein), however, there is only a few studies on TM decorated graphynes.

Stimulated by the synthesis of graphdiyne nanowires [27], Lin *et al.* studied the adsorption and diffusion of Au, Cu, Fe, Ni, and Pt adatoms on a graphdiyne nanoribbon [28] by DFT calculations using the Perdew-Burke-Ernzerhof (*PBE*) exchange-correlation functional [29]. They predicted *n*-doping when Fe, Ni, and Pt are adsorbed and a metallic character in the case of Au and Cu adatoms, without significant effect on the graphyne band structures. On the other hand, Alaei and coworkers studied Fe, Co, and Ni adsorption on γ-graphyne nanotubes [30] by DFT calculations using PBE functional, given that such structures were experimentally observed [31]. They showed how adsorption of Fe and Co affects the magnetism of the graphyne nanotubes, while all adatoms resulted in *n*-doped graphyne nanotubes.

Graphynes have been used in heterogeneous catalysis due to their appealing large specific surface areas, 3440 $m^2 g^{-1}$ for γ-graphyne [32]. The CO oxidation catalyzed by Sc and Ti single atoms supported on graphdiyne has been reported [33]. Azizi *et al.* explored the interactions of Au adatoms as well as gold dimers and trimers on a γ-graphyne model by DFT [34] calculations. The field, yet maturing, is still in its infancy, and the so far performed research is driven mostly by chemical intuition. A clear and defined theoretical background is necessary to address further research on specific interesting property targets, and also in order to avoid erratic research. In this context, we here consistently explored the adsorption and diffusion of all 3*d*, 4*d*, and 5*d* TMs on γ-graphyne by DFT with PBE exchange-correlation functional including dispersive interactions through the Grimme D2 correction [35]. This particular graphyne has been chosen as a textbook representative since it is robust [36], displays both benzene and acetylenic rings (see Fig. 2), and allows for comparison with previous studies [34] and also with graphene [26]. Structural changes, doping, and inferred magnetism are systematically studied in full, paving the way for further application-driven research.

2. Computational Details

Spin polarized DFT calculations have been performed using the Vienna *Ab initio* Simulation Package —VASP [37]. The Projector Augmented Wave (*PAW*) method has been used to represent atomic cores effect on the valence electron density [38]. This simulation of the core states allows one to obtain converged results —energy variations below 0.001 eV— with a cut-off kinetic energy of 415 eV for the plane-wave basis set. Geometry optimizations were performed using a conjugated gradient algorithm and applying a first-order Methfessel-Paxton smearing of 0.2 eV width, yet final energies were corrected to 0 K (no smearing). The convergence threshold for the total energy was set to 10^{-5} eV and structural optimizations were finalized when forces acting on atoms were below 0.01 eV $Å^{-1}$. All DFT calculations have been carried out using the PBE exchange-correlation (*xc*) functional [29], a representative of Generalized Gradient Approximation (*GGA*) ones. PBE values provide an optimized pristine γ-graphyne rhombohedral lattice structure with unit cell parameters of 6.880 Å (*i.e., a = b*), in very good agreement with previous calculations [36,39]. PBE yields the best overall description of TMs among many Local Density Approximation (*LDA*), GGA, meta-GGA, and hybrid xc functionals [40,41].

Energy and structure optimizations have been carried out on a *p*(2×2) slab supercell, since it grants a separation between adsorbed adatoms of ~1.3 nm, enough to avoid interactions with TM adatoms on periodically repeated adjacent cells. According to test calculations lateral interactions are estimated to be below 0.02 eV. For this supercell size the TM atomic coverage is ~0.02 ML. The optimized γ-graphyne cell parameters when adsorbing a TM atom revealed little structural changes, below 3%, and so have been disregarded in the following. A vacuum region of 1 nm is added along the direction normal to the γ-graphyne layer, in order to avoid interactions between repeated slabs. Test calculations with double

vacuum yielded variations in the energy of ~0.003 eV. An optimal Monkhorst-Pack [42] **Γ**-centred **k**-point grid of 2×2×1 dimensions was used.

The van der Waals (vdW) dispersive interaction is accounted *via* D2 dispersion correction of Grimme [35]. This particular correction has been found to be one of the best choices for the interaction of graphene with TM surfaces [43,44], as well as the correction of choice in an earlier study [33]. Dispersion coefficients, C_6, and vdW radii, R_0, for 3*d* and 4*d* TMs were collected from the original paper [35], and those for 5*d* metals from a later study [45]. Test calculations on selected systems using Grimme D3 correction [46] or many body dispersion (MBD) [47] yielded similar results, thus, the overall picture seems not to be biased by the chosen van der Waals description. For comparative purposes with previous work on graphene we restricted the discussion to D2.

For any TM atom adsorbed on γ-graphyne the adsorption energy, E_{ads}, is defined as

$$E_{ads} = (E_{GY} + E_{TM}) - E_{TM/GY} \quad (1),$$

where $E_{TM/GY}$ is the total energy of γ-graphyne layer with the TM adatom attached, E_{GY} is the total energy of the pristine γ-graphyne layer, and E_{TM} the total energy of an isolated TM atom as previously calculated [40]. Thus, adsorption energies are defined positive, and therefore, the larger the E_{ads} value, the stronger the interaction between γ-graphyne and the TM atom. Charges on TM adatoms, *Q*, which are necessarily related to the oxidation state, have been estimated through a Bader analysis of the electron density [48]. Adatom height, *h*, has been calculated with respect to the mean plane of the γ-graphyne sheet, see Figure 1. The γ-graphyne corrugation, *c*, has been estimated by subtracting the height of the highest C atom from that of the lowest, and defining it positive whenever the γ-graphyne layer approaches to the TM adatom, *i.e.* forming a hill where TM adatom sits atop, and, *vice versa*, negative whenever γ-graphyne is repelled from the TM adatom, forming a valley which embraces the TM adatom, see Figure 1.

Fig. 1. Schematic representation of the structural parameters under analysis, including the TM atom height (h) over the average height of the C atoms of γ-graphyne, and the corrugation, c, obtained as the difference in height of the upmost and bottommost C atoms in γ-graphyne. The sketched case belongs to a positive c value. Carbon atoms are represented by green spheres, and the TM by a yellow sphere.

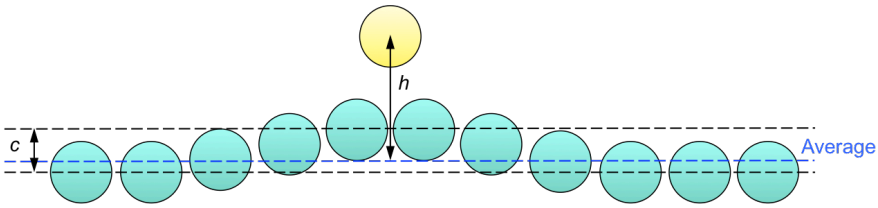

Adatom diffusion is a vital process in its tethering to a surface and to the related cluster formation processes. Because of this diffusion, transition states have been obtained in a point-wise fashion where the adatom plane position is kept fixed, as well as that of the underlying C atoms, whereas all other degrees of freedom are allowed to relax. In this way, sliding or deformation of the γ-graphyne to accommodate the TM adatom or to displace it to a minimum is avoided. Minima and Transition States (*TS*) have been characterized by all positive and only one imaginary vibrational frequency, respectively, obtained from the diagonalization of the Hessian matrix by finite differences of analytical gradients with individual displacements of 3 pm in each cell direction.

3. Results and Discussion

For the adsorption of TM atoms on γ-graphyne we considered various high-symmetry adsorption sites including Top (T), Bridge (B), and Hollow (H) sites. For each adsorption site type, differently from graphene [26], there are several specific sites as depicted in Fig. 2. For example, there are top sites on the benzene ring (T_1) and on a C site of an acetylenic linkage

(T_2). Concerning bridge sites between two atoms, there is one on the benzene ring (B_1), one linking a benzene ring and an acetylenic linkage (B_2), and finally a bridge at the acetylenic link (B_3). Two main different hollow sites are contemplated, above the acetylenic ring (H_1) and over the benzene ring (H_2). Finally, a γ-graphyne in-plane situation is contemplated, in which TM atom is placed inside the acetylenic ring (H_3). Note that other lower symmetry sites have not been sampled, yet on graphene were found not to be occupied [26].

Fig. 2. Schematic representation of the adsorption sites of a TM atom on γ-graphyne — labelled yellow spheres— from a top view (top image), and also the in-plane situation for H_3 and its relationship with H_1 site from a side perspective (bottom image). Carbon atoms correspond to green spheres.

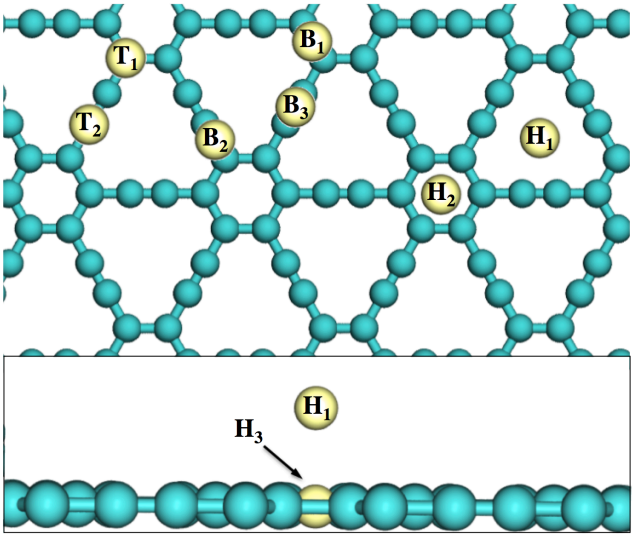

For each TM adatom, the most stable site and its adsorption energy, the TM height from the γ-graphyne sheet (h), the graphyne layer corrugation (c), the TM diffusion energy barrier (E_{dif}), the TM charge (Q) triggered by a TM→γ-graphyne charge transfer, the variations on TM adatom magnetic moment ($\Delta\mu$), and the overall local magnetic moment (μ) are listed in Table 1. The same results obtained from PBE-D2 including the dispersive interactions are listed in Table 2.

Table 1: Summary of PBE results for 3*d*, 4*d*, and 5*d* TM on γ-graphyne including most stable adsorption site, adsorption energy, E_{ads}, diffusion energy barrier, E_{dif} (TS location in parenthesis), TM height from γ-graphyne, *h*, γ-graphyne corrugation, *c*, TM adatom net charge, *Q*, total magnetic moment, μ, and magnetic moment variation with respect to isolated TM atom, $\Delta\mu$. Energies are in eV, distances in Å, *Q* in *e*, and μ and $\Delta\mu$ are given in μ_B.

TM	Site	E_{ads} /eV	*h* /Å	*c* /Å	*Q* /e	$\Delta\mu$ /μ_B	μ /μ_B	E_{dif}/eV
Sc	H_1	4.11	1.14	0.07	1.55	-1.00	0.00	0.86 (B_2)
Ti	H_1	4.79	1.43	0.07	1.48	-2.00	0.00	1.77 (B_2)
V	H_1	4.84	1.24	0.06	1.24	-2.18	0.82	2.18 (B_2)
Cr	H_1	2.56	1.03	0.06	1.11	-4.11	1.89	1.58 (B_3)
Mn	H_1	3.20	0.83	0.06	0.99	-2.00	3.00	2.21 (B_3)
Fe	H_1	4.23	0.62	0.04	1.04	-1.93	2.07	2.75 (B_3)
Co	H_3	5.02	0.09	0.01	0.67	-2.00	1.00	3.03 (B_3)
Ni	H_3	5.31	0.07	-0.01	0.64	-2.00	0.00	3.08 (B_3)
Cu	H_3	3.34	0.07	-0.01	0.63	-1.00	0.00	2.38 (B_3)
Zn	H_2	0.02	3.85	0.00	0.02	0.00	0.00	0.00 (T_2)
Y	H_1	4.12	1.31	0.07	1.70	-1.00	0.00	0.86 (B_2)
Zr	H_1	5.26	1.72	0.08	1.57	-2.00	0.00	1.55 (B_2)
Nb	H_1	5.51	1.49	0.07	1.44	-5.00	0.00	2.71 (B_2)
Mo	H_1	4.22	1.33	0.07	1.06	-4.69	1.31	2.82 (B_3)
Tc	H_1	4.34	1.22	0.07	0.83	-3.01	1.99	2.32 (B_3)
Ru	H_1	4.25	1.10	0.06	0.58	-1.54	2.46	2.07 (B_3)
Rh	H_1	4.15	0.85	0.07	0.38	-2.00	1.00	1.58 (B_3)
Pd	H_1	2.70	0.48	0.05	0.47	0.00	0.00	1.06 (B_3)
Ag	H_1	0.95	1.57	0.03	0.54	-1.00	0.00	0.59 (T_2)
Cd	T_2	0.03	3.93	-0.01	0.02	0.00	0.00	0.00 (H_1)
La	H_1	5.03	1.51	0.07	1.66	-1.00	0.00	0.52 (B_2)
Hf	H_1	5.07	1.69	0.08	1.77	-2.00	0.00	2.05 (T_2)
Ta	H_1	6.10	1.52	0.08	1.53	-2.51	0.49	3.13 (B_2)
W	H_1	6.14	1.36	0.07	1.25	-2.74	1.26	3.66 (B_3)
Re	H_3	2.99	0.00	0.00	1.82	-2.01	2.99	2.35 (B_2)
Os	H_1	5.04	1.08	0.07	0.98	-2.07	1.93	3.91 (B_3)
Ir	H_1	4.96	0.79	0.07	0.64	-2.03	0.97	2.19 (B_3)
Pt	H_1	4.23	0.45	0.05	0.48	-2.00	0.00	1.78 (B_3)
Au	H_1	1.02	0.49	0.05	0.50	-1.00	0.00	0.39 (T_2)
Hg	T_1	0.02	4.11	0.00	0.01	0.00	0.00	0.00 (B_1)

Table 2: Summary of PBE-D2 calculated results for 3*d*, 4*d*, and 5*d* TM on γ-graphyne including the most stable adsorption site. Reported properties and units are as in Table 1.

TM	Site	E_{ads} /eV	*h* /Å	*c* /Å	*Q* /e	$\Delta\mu$ /μ_B	μ /μ_B	E_{dif}/eV
Sc	H_1	4.30	1.15	0.07	1.55	-1.00	0.00	0.87 (B_2)
Ti	H_1	5.00	1.42	0.07	1.47	-2.00	0.00	1.77 (B_2)
V	H_1	5.06	1.24	0.06	1.24	-2.19	0.81	2.18 (B_2)
Cr	H_1	2.78	1.04	0.06	1.11	-4.11	1.89	1.59 (B_3)
Mn	H_1	3.39	0.82	0.05	0.99	-2.00	3.00	2.22 (B_3)
Fe	H_1	4.42	0.61	0.04	1.03	-1.92	2.08	2.95 (B_3)
Co	H_3	5.20	0.00	0.00	0.69	-2.00	1.00	3.03 (B_3)
Ni	H_3	5.48	0.06	0.00	0.64	-2.00	0.00	3.19 (B_3)
Cu	H_3	3.51	0.07	0.01	0.64	-1.00	0.00	2.37 (B_3)
Zn	H_1	0.15	2.99	0.00	0.00	0.00	0.00	0.02 (B_2)
Y	H_1	4.39	1.31	0.07	1.69	-1.00	0.00	0.62 (B_2)
Zr	H_1	5.54	1.72	0.08	1.56	-2.00	0.00	1.56 (B_2)
Nb	H_1	5.79	1.48	0.07	1.44	-5.00	0.00	2.93 (B_2)
Mo	H_1	4.49	1.33	0.07	1.05	-4.69	1.31	2.70 (B_2)
Tc	H_1	4.60	1.23	0.07	0.86	-3.01	1.99	2.54 (B_3)
Ru	H_1	4.51	1.10	0.06	0.59	-1.54	2.46	2.34 (B_3)
Rh	H_1	4.39	0.88	0.07	0.38	-2.00	1.00	1.57 (B_3)
Pd	H_1	2.93	0.48	0.05	0.47	0.00	0.00	1.04 (B_3)
Ag	H_1	1.25	1.58	0.03	0.54	-1.00	0.00	0.66 (T_2)
Cd	H_1	0.20	3.01	0.00	0.03	0.00	0.00	0.03 (B_2)
La	H_1	5.28	1.50	0.07	1.66	-1.00	0.00	0.52 (B_2)
Hf	H_1	5.36	1.69	0.08	1.77	-2.00	0.00	1.99 (T_2)
Ta	H_1	6.51	1.52	0.08	1.53	-2.51	0.49	3.27 (T_2)
W	H_1	6.41	1.36	0.07	1.24	-2.74	1.26	3.65 (B_3)
Re	H_3	3.12	0.00	0.00	1.82	-2.01	2.99	2.28 (B_2)
Os	H_1	5.27	1.07	0.08	0.98	-2.08	1.92	2.54 (B_3)
Ir	H_1	5.10	0.84	0.07	0.64	-2.01	0.99	2.14 (B_3)
Pt	H_1	4.50	0.44	0.05	0.48	-2.00	0.00	1.71 (B_3)
Au	H_1	1.24	0.36	0.04	0.51	-1.00	0.00	0.34 (T_2)
Hg	H_1	0.27	2.92	0.00	0.03	0.00	0.00	0.02 (H_2)

3a. Energetic Properties

Let us begin with the two energetic properties under investigation, namely, the adsorption strength, E_{ads}, and the diffusion energy barrier among adsorption sites, E_{dif}. It is worth to note, beforehand, that, as seen in Table 1, most of TMs prefer to adsorb over the acetylenic ring (H_1), except Co, Ni, Cu, and Re, which prefer to adsorb at H_3 site. Indeed it appears as atomic size plays a key role, as far as the reduced vertical height (h) on H_1 site when moving along a *d* series is consistent with a reduction of the atomic radii. Co, Ni, and Cu, being the smallest TMs, fit inside the acetylenic ring. In spite of its small size, however, Zn is adsorbed at H_2 site due to its very weak interaction, being essentially physisorbed. Re is an exceptional case because it features a high interaction with γ-graphyne at H_3 site despite its larger atomic radius.

It was reported that Au was adsorbed at in-plane site, *i.e.* H_3, on γ-graphyne [34], and Fe, Co, and Ni at H_3 on γ-graphyne nanotubes [30]. In this study, Fe was adsorbed at H_1 site on γ-graphyne, but with a reduced height of 0.62 Å. The tension on the wrapped γ-graphyne nanotube could account for such a small difference. Similarly, the adsorption of Au on γ-graphyne molecular flake allowed for further lateral displacement of the acetylenic linkages to better accommodate the Au atom in-plane [34]. Indeed, a larger acetylenic ring may favour in-plane situations as seen in graphdiyne, where Au naturally places in-plane in the equivalent H_3 position [28] even when displaying periodic boundary conditions. Other TMs (Sc, Ti, Cu, Fe, Ni, Pt) in graphdiyne place at the acetylenic ring, but displaced towards the benzene, what here is called the benzene-acetylenic pocket [28,33].

The binding strengths along the *d* series are plotted in Fig. 3. First thing to notice is the rather large binding energies of TMs adsorbed on γ-graphyne. Values of E_{ads} can be as high as 5.26 eV as obtained for Zr on H_1 at PBE level, and sensibly larger than equivalent values on graphene, with a reported value at same computational level of 2.11 eV for Zr on a Hollow

site [26]. The calculated adsorption energy values approach the TM bulk cohesive energies reported in a comparable previous study [40], even slightly larger for two cases (Ni and La), indicating a thermodynamically driven atomic dispersion. However, for the other TMs this points for a less pronounced tendency to aggregation compared to results on graphene substrate [26].

The high E_{ads} values for TMs on γ-graphyne compared with graphene are probably due to the γ-graphyne metastability itself. The reduced C coordination and the concomitant higher reactivity of *sp* C atoms are responsible for the higher chemical activity of γ-graphyne, resulting in stronger attachment of adatoms. This explanation is in line with an enhanced electrophilic activity at the acetylenic ring centre of γ-graphyne and stronger attachment of TMs upon it [34]. Present PBE estimated E_{ads} (1.02 eV) for Au on γ-graphyne is in perfect line with a previous report of 1.1 eV [34]. However, E_{ads} values for Fe (4.23), Co (5.02), and Ni (5.31) on γ-graphyne are slightly larger (~0.2-0.4 eV) than those obtained on γ-graphyne nanotubes of 4.58, 4.83, and 4.93 eV, respectively, which seems to indicate that nanotube curvature may reduce the TM attachment strength [30].

It is interesting to compare with graphdiynes, where a further lengthening of the acetylenic linkages increases the TM attachment strength. For instance, the adsorption energies of Sc and Ti on graphdiyne were obtained to be 6.07 and 6.43 eV at PBE level [33], whereas those on γ-graphyne are found here to be 4.11 and 4.79 eV, respectively. The adsorption energies for late TMs on graphdiyne previously reported for Au (3.4), Cu (4.6), Fe (7.4), Ni (7.7), and Pt (5.1 eV) are ~1-3 eV larger than present values on γ-graphyne, see Table 1.

As far as trends are considered, Fig. 3 shows the camel humps shape of adsorption energies for TMs on γ-graphyne, which is reminiscent of what featured on graphene [26], mainly originated from the low attachment strength of more stable d^5 and d^{10} elements.

Indeed, d^{10} elements of group XII feature rather weak binding energies with physisorption, and other vicinal d^{10} elements such as Cu, Pd, Ag, and Au show also a reduced adsorption energy, yet their E_{ads} values of ~1 eV or higher assign their adsorption as chemisorption. Similarly, d^5 TMs such as Cr, Mn, Mo, and Re show reduced E_{ads} values compared to d^4 and d^6 TMs, hence the hump shape is still observed in Fig. 3, although the trend is deviated from that on graphene in that d^5 TMs are strongly adsorbed with E_{ads} values above 2.6 eV.

The trends obtained by PBE description seem to be unchanged by explicitly including the dispersive interaction (PBE-D2). Largest change is observed on group XII d^{10} TMs, which, according to PBE-D2 calculations, occupy H_1 positions, in line with the majority of other TMs. However their E_{ads} values (among 0.15-0.27 eV) are still modest, see Table 2, and physisorption character is kept. These TMs are located closer to the γ-graphyne plane, about 1 Å, from the PBE-D2 results, see *h* values in Tables 1 and 2. Generally, the role of dispersive forces on the rest of TMs could be considered secondary, though adsorption strengths are systematically increased by 0.13-0.41 eV and TM heights essentially untouched, with variations in the order of 0.01 Å. Only somewhat larger displacements are found for Co and Au. Co positions in-plane allocation by downshifting *h* from 0.09 Å to 0.00 Å. Au approaches towards the γ-graphyne plane by *h* reduction of 0.13 Å, yet it is still located out-of-plane (H_1).

The other very significant difference for TMs adsorbed on γ-graphyne compared to graphene is the diffusion energy barriers, E_{dif}. Most TSs are located over acetylenic bridges B_2 and B_3, see Table 1, connecting vicinal H_1 or H_3 sites. For such TMs, the diffusion energy barrier values obtained by PBE are rather high, ranging from 0.52 (La) to 3.91 eV (Os), which are much larger than on graphene ranging from 0.00 (Re) to 0.69 eV (Ta) [26]. Indeed the enhanced adsorption strength on γ-graphyne is directly linked to the acetylenic ring, which in turn enlarges the diffusion energy barriers. Accordingly, the combination of high adsorption

energy close to the cohesive energies of bulk TMs and high diffusion energy barrier would make adatoms rather immobile over the γ-graphyne. The calculated diffusion energy barriers for Fe, Co, and Ni of 2.75, 3.03, and 3.08 eV, respectively, are comparable with values of ~3.1 eV for diffusion over B_3 sites on γ-graphyne nanotubes [30].

The exceptions to this are groups XI and XII; the diffusion of group XII TMs is barrierless due to their rather weak adsorption. Group XI TMs Ag and Au present diffusion over T_2, with sensibly small diffusion energy barriers of 0.59 and 0.39 eV, respectively, which implies an easy diffusion at room temperature. These results agree with smaller diffusion energies for Au on graphdiyne of 1.3 eV, compared to those for Fe, Ni, and Pt, which were reported to be 3.3, 2.7, and 2.0 eV, respectively [28]. Finally, the double hump trend for E_{ads} is somewhat followed for E_{dif}, yet less pronounced, also at variance with what was found on graphene [26]. It is worth to stress out also the relatively low E_{dif} values of group III TMs of 0.86 (Sc), 0.86 (Y), and 0.52 eV (La), which could point also for an easy diffusion at room temperature.

Effect of vdW forces on diffusion energy barriers is also rather modest with fluctuations below 0.1 eV though the effect is more remarkable in some particular cases. For instance, the diffusion energy barrier for Fe is increased by 0.2 eV when including vdW, see Table 2, whereas reduced by 0.24 eV for Y. For middle 4*d* metals Nb, Mo, Tc, and Ru, vdW increased the diffusion energy barrier by ~0.2-0.3 eV. For Os, the diffusion barrier 3.91 eV obtained by PBE was remarkably reduced to 2.54 eV by PBE-D2.

Fig. 3. Adsorption energy (E_{ads}) of 3*d*, 4*d*, and 5*d* TM atoms on γ-graphyne, as well diffusion energy barriers, E_{dif}, both in eV. Shown are the PBE (open circles and solid lines) and PBE-D2 (filled circles and dashed lines) results.

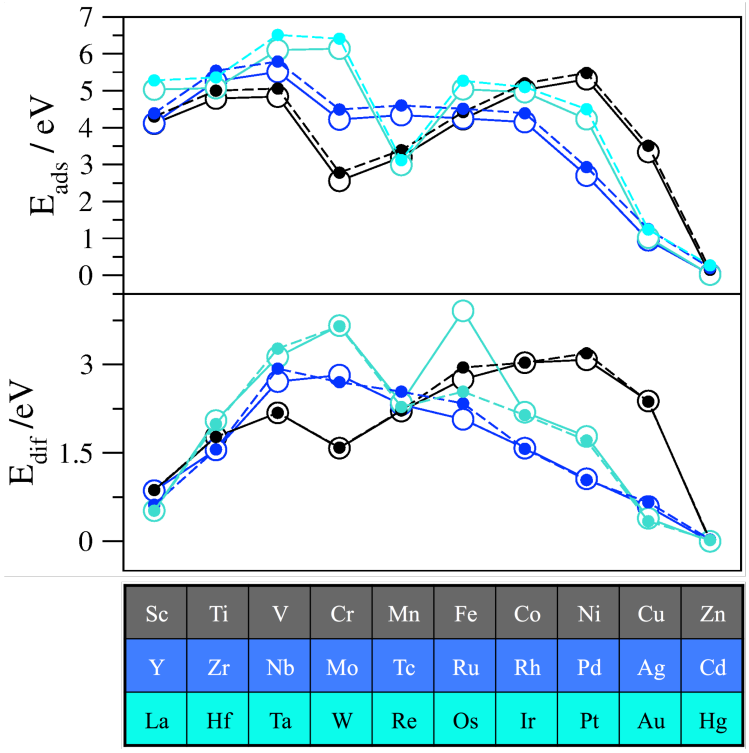

3b. Structural Properties

As above briefly commented, TM adatoms prefer, in general terms, to adsorb on H_1 position, with the caveats of Co, Ni, Cu, and Re which prefer to adsorb in a H_3 site. Group XII TMs Zn, Cd, and Hg seem to have a slight preference for H_1, see Table 2. The H_1 or H_3 preference is mainly due to strong covalent bonds between the *sp* C atoms at the acetylenic linkages and the central TM adatom. Furthermore, Fig. 4 evidences that for any series the height of the TM adatom over the H_1 adsorption site reduces when moving along a *d* series, in line with its atomic radius reduction. Thus, the smaller the radius, the closer is the TM to an in-plane H_3 position. Obviously, TMs positioned at H_3 sites disobey the trend, as their nominal height *h* is zero. Slight tendency outliers are group III TMs Sc, Y, and La, whose

height is somewhat lower than expected, and the opposite applies for Au. Silver case is worth mentioning, as it displays a height clearly larger than other TMs, a point that goes along with a reduced adsorption energy of 0.95 eV as obtained at PBE level. Finally, as aforementioned, group XII TMs Zn, Cd, and Hg are placed at a height *circa* 4 Å in consistency with the physisorbed situation. However, this rather large height is lowered by ~1 Å when including vdW forces, see values in Table 2. As also stated above, Au and Co reduced slightly their heights when carrying out PBE-D2 calculations.

As far as corrugation *c* values are concerned, they are rather small, showing a slightly positive value, which is translated in an approaching of the C atoms of γ-graphyne towards the TM adatom (Fig. 4). Notice that *c* values are less than 0.08 Å, which are sensibly smaller than those on graphene, where in some cases corrugations of up to 0.3 Å were found [26]. Indeed, this difference of behaviour is closely related to the structure of γ-graphyne. The acetylenic linkages and the acetylenic ring space allow for an in-plane relaxation in the course of TM adatom accommodation, a factor inexistent in graphene, and linked to the C *sp* lower degree of coordination [49]. Last but not least, vdW effect on such small degree of relaxation could be negligible, being its impact, at most, of 0.01 Å in few cases.

Fig. 4. Adsorption height, *h*, of 3*d*, 4*d*, and 5*d* TM adatoms on γ-graphyne as well as its corrugation, *c*, both in Å. Shown are the PBE (open circles and solid lines) and PBE-D2 (filled circles and dashed lines) results.

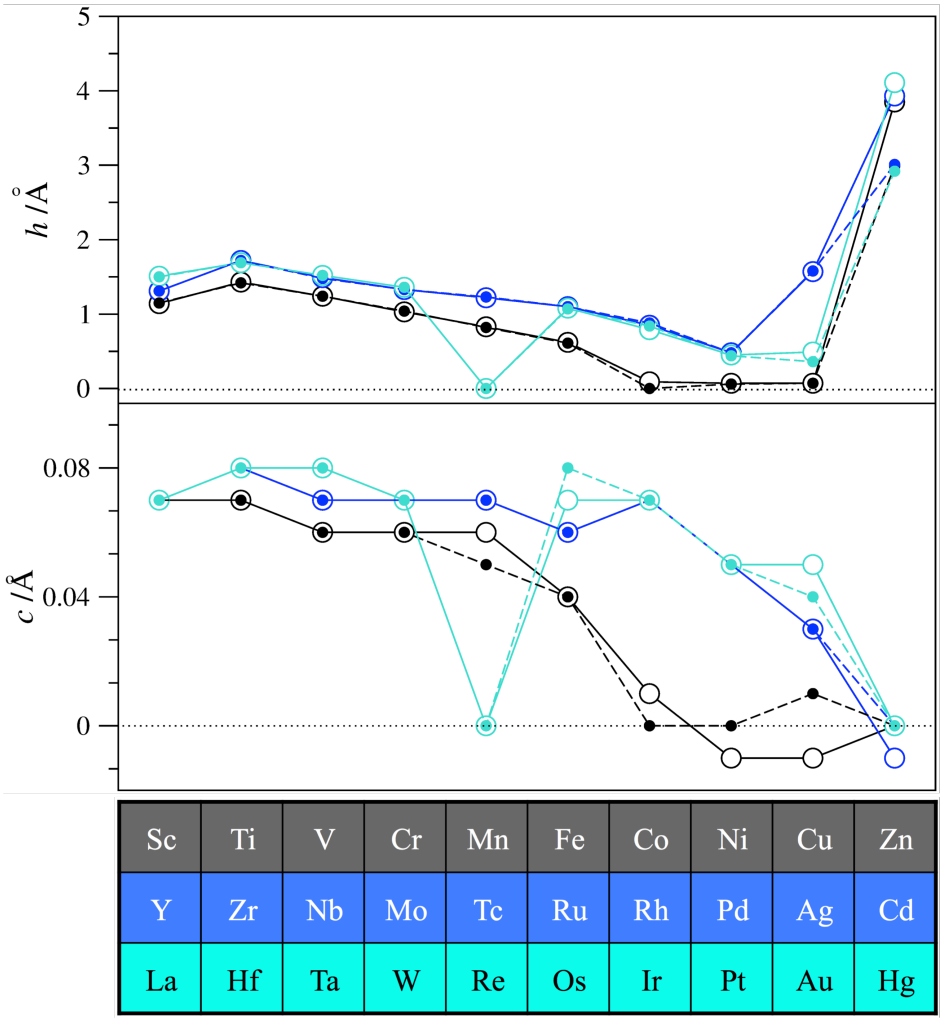

3c. Electronic and Magnetic Properties

Finally, electronic and magnetic properties are here addressed. The net charges obtained through a Bader analysis are plotted in Fig. 5. As clearly seen in Fig. 5, all TMs transfer electron density to the γ-graphyne layer, similar to the overall trend on graphene [26]. The result is otherwise opposed to a suggested electron density donation from γ-graphyne to *d* and *s* orbitals of the TM adatom [34]. Note that the charge transfer is more acute for early TMs, and more attenuated for late TMs, easily explained based on Pauling electronegativities, which reduces along *d* series.

Present results go along with previous simulations; Azizi *et al.* [34] highlight a charge of 0.88 *e* on adsorbed Au, according to Mulliken population, a result comparable to present

value of 0.50 *e* from a Bader analysis. Furthermore present values of Bader charges for Fe, Co, and Ni of 1.04, 0.67, and 0.64 *e* compare well to the values obtained on γ-graphyne nanotubes of ~0.8-0.9 *e* [30]. The extent of the charge transfer is clearly larger than on graphene, when comparing present results to previous equivalent results [26]. Charge transfer enhancement can be as high as 1.8 *e* for Re or 1.1 *e* for V, or more moderate of 0.1 *e* for Ru and Rh. In any case the *n*-doping by TM atom adsorption is clear, and the trend could serve to modulate the amount of doping. A note has to be put on Re, in which the H_3 occupation seems to be the origin of a higher charge transfer to γ-graphyne hence of a higher oxidation state of the trapped TM. Note as well that the vdW effect on TM oxidation states is minimal, see Fig. 5. Indeed, the acidic isolated nature of the TM adatoms could well be at the origin of a given desired catalytic activity, such as the suggested CO oxidation efficiency of Sc and Ti adatoms on graphdiyne [33].

Aside from that it is important to highlight that, excluding group XII TMs, any TM adatom on γ-graphyne would be positively charged, and so, coulombic repulsion among such cations would also presumably kinetically inhibit their aggregation. This factor adds up to the aforementioned adsorption energy close to the bulk TM cohesive energy and to the overall high diffusion energies in stating the possibility of having isolated TM adatoms on γ-graphyne. In two cases, Ni and La, such a situation seems to be thermodynamically driven. However, for group XII TMs Zn, Cd, and Hg, the low binding energy, low diffusion energy barriers, and low charge transfer seem to indicate an easy and rapid aggregation.

Fig. 5. Oxidation state (Q), local magnetic moment (μ), and variation of the atomic magnetic moment ($\Delta\mu$) of 3*d*, 4*d*, and 5*d* TM adatoms on γ-graphyne. Units are as in Tables 1 and 2. Shown are the PBE (open circles and solid lines) and PBE-D2 (filled circles and dashed lines) results.

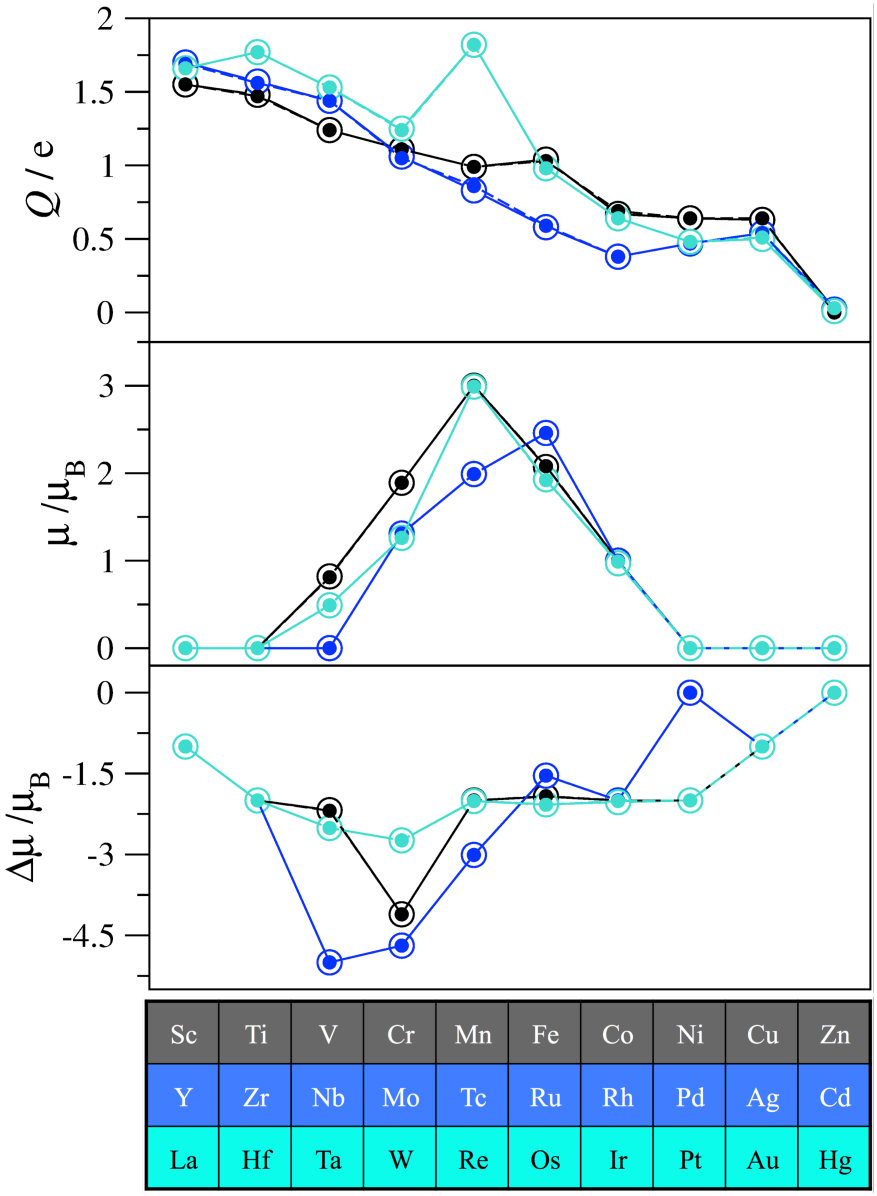

Finally, we have examined the local magnetic moment, μ, along the *d* series. As clearly observed in Fig. 5, a volcano trends arises, where magnetic moment is heavily quenched for early groups III and IV, and as well to late groups X and XI, differently from graphene, where magnetic moment was even enhanced for early TMs and survived in group XI TMs. In these cases, TM/γ-graphyne composite would behave as a diamagnetic material. Clearly, the overall strong interaction of TMs with γ-graphyne quenches their magnetic moment, partly due to the larger charge transfer to the γ-graphyne bandstructure, where α and

β spins couple, partly to orbital mixing of *d* orbitals of TMs and conduction band of γ-graphyne. However, significant magnetic moments are found for groups V-IX, with a maximum obtained for d^5 elements, which would be better suited to bestow magnetism to γ-graphyne sheets. The calculated μ values for Fe, Co, and Ni of 2.07, 1.00, and 0.00 μ_B are in perfect agreement with corresponding values of 2.06, 1.00, and 0.01 μ_B obtained on γ-graphyne nanotubes [30].

The magnetic quenching is easily observed through the $\Delta\mu$ evolution along *d* series (Fig. 5). The stronger reduction for early TMs, a moderate reduction in middle TMs, and a somewhat lower reduction for late TMs are clearly observed. The reduction of magnetism well explains the volcano plot of μ, and highlights the different magnetic behaviour of γ-graphyne compared to graphene [26]. As happened with μ, the addition of vdW description has little effect on the magnetic reduction.

4. Conclusions

Adsorption of transition metal atoms on graphynes constitutes an attractive way of modifying their electronic and magnetic properties, with implications in spintronics and nanomagnetism. Aside, the functionalization of graphynes by TM adatoms may have repercussions in molecular storage, such as for H_2, sensing, and, furthermore, these adatoms can be active centres of envisioned graphyne-supported catalysts. Here we provide a thorough density functional theory study of the structural, energetic, diffusivity, magnetic, and electronic properties for the full sets of 3*d*, 4*d*, and 5*d* TM adatoms adsorbed on γ-graphyne, an experimentally reported graphyne representative featuring both acetylenic rings and linkages characteristic of graphynes family, but also benzene-like rings characteristic of graphene, allowing for comparison. The study is complemented by explicitly including vdW forces in the interaction description, thus weighting their relative importance. TM adatoms

have been systematically sampled on all high adsorption sites including top, bridge, and hollow sites, plus evaluating as well the diffusion among them.

Transition metal adatoms are found to, in general terms, sit on H_1 sites over γ-graphyne acetylenic rings, yet Co, Ni, and Cu, due to their reduced atomic radii, place themselves in-plane of the acetylenic rings, in the H_3 hollow, as well as for Re. Atomic radius is indeed found to play a key role in determining the height over the acetylenic ring. For group XII d^{10} TMs, a weak physisorption over multiple sites is suitable, with a rather easy diffusion being essentially a barrierless process. For the rest of the TMs, the adsorption strength is rather high, ranging ~1-6 eV, instigated by the metastability of γ-graphyne, and also displaying rather high diffusion energy barriers of ~0.5-3.5 eV. For group XII TMs, adatoms are located at a height of ~ 3 Å as gained at PBE-D2 level, whereas the rest of TM adatoms are located ~ 0.4-1.7 Å above H_1 sites, and with a height of nominally zero for in-plane H_3 sites. The γ-graphyne sheet is found not to be deformed out-of-plane when adsorbing TMs, as acetylenic linkages can deform in-plane to accommodate TM adatoms. In all the studied cases, TMs are found to quite substantially *n*-dope γ-graphyne by charge transfer, and trend along *d* series is governed by the TM Pauling electronegativity. Some TM adatoms do also bestow magnetism to the resulting composite, specially the middle ones, as local magnetic moments are heavily quenched for early and late TMs due to the strong adsorption. Except for the group XII TMs weakly adsorbed adatoms, vdW forces are found to play overall a minor role in the adsorption and diffusion of the adatoms, as well as on their electronic and magnetic properties.

Comparison of present results on γ-graphyne with equivalent results on graphene evidence a much stronger TM attachment, larger diffusion barriers, and a stronger charge transfer to the γ-graphyne. Indeed, adsorption energies close to the bulk TM cohesive energies, the diffusion energy barriers above 1 eV, and the coulombic repulsion among

positively charged TM adatoms are three ingredients. These suggest a possible isolated atom situation at moderate conditions of temperature, given that aggregation would be kinetically inhibited. This has concomitant interest in using isolated TM atomic centres in heterogeneous catalysis, or as magnetic pinpoints on graphyne based nanodevices. Present results hence provide a solid theoretical ground for further research on γ-graphyne in particular, but on graphyne family in general, from which results can be envisaged and/or interpreted from.

Acknowledgements

The work at SKKU was supported by the NRF (No. 2016R1A2B4012337) of Korea government (Ministry of Science, ICT & Future Planning), and the computing resource at SKKU was supported by the KISTI supercomputing center through the strategic support program for the supercomputing application research [No. KSC-2015-C1-040]. The work at UB by Spanish *Ministerio de Economía y Competitividad* grants (CTQ2014-53987-R and CTQ2012-30751) and *Generalitat de Catalunya* grants (2014SGR1582, 2014SGR97, and XRQTC). P.G. thanks Generalitat de Catalunya for his Serra Húnter Associate Professorship. F.V. thanks the Spanish *Ministerio de Economía y Competitividad* for the *Ramón y Cajal* (RyC) postdoctoral grant (RYC-2012-10129).

References

[1] Y. Li, L. Xu, H. Liu, Y. Li, Graphdiyne and graphyne: from theoretical predictions to practical construction, Chem. Soc. Rev. 43 (2014), 2572-2586.

[2] V. Georgakilas, J.A. Perman, J. Tucek, R. Zboril, Broad Family of Carbon Nanoallotropes: Classification, Chemistry, and Applications of Fullerenes, Carbon Dots, Nanotubes, Graphene, Nanodiamonds, and Combined Superstructures, Chem. Rev. 115 (2015) 4744-4822.

[3] A.L. Ivanovskii, Graphynes and Graphdyines, Prog. Solid State Chem. 41 (2013) 1-19.

[4] A.T. Balaban, C.C. Rentia, E. Ciupitu, Estimation of Relative Stability of Several Planar and Tridimensional Lattices for Elementary Carbon, Rev. Roum. Chim. 13 (1968) 231-247.

[5] R.H. Baughman, H. Eckhardt, M. Kersetz, Structure-property predictions for new planar forms of carbon: Layered phases containing sp^2 and *sp* atoms, J. Chem. Phys. 87 (1987) 6687.

[6] D. Malko, C. Neiss, F. Viñes, A. Görling, Competition for Graphene: Graphynes with Direction-Dependent Dirac Cones, Phys. Rev. Lett. 108 (2012) 086804.

[7] J. Chen, J. Xi, D. Wang, Z. Shuai, Carrier Mobility in Graphyne Should Be Even Larger than That in Graphene: A Theoretical Prediction, J. Phys. Chem. Lett. 4 (2013) 1443-1448.

[8] Z. Li, M. Smeu, A. Rives, V. Maraval, R. Chauvin, M.A. Ratner, et al., Towards graphyne molecular electronics, Nat. Commun. 6 (2015) 6321.

[9] M. Long, L. Tang, D. Wang, Y. Li, Z. Shuai, Electronic Structure and Carrier Mobility in Graphdiyne Sheet and Nanoribbons: Theoretical Predictions, ACS Nano 5 (2011) 2593-2600.

[10] S. Wang, L. Yi, J.E. Halpert, X. Lai, Y. Liu, H. Cao, et al., A Novel and Highly Efficient Photocatalyst Based on P25-Graphdiyne Nanocomposite, Small 8 (2012) 265-271.

[11] N. Yang, Y. Liu, H. Wen, Z. Tang, H. Zhao, Y. Li, et al., Photocatalytic Properties of Graphdiyne and Graphene Modified TiO_2: From Theory to Experiment, ACS Nano 7 (2013) 1504-1512.

[12] G. Li, Y. Li, H. Liu, Y. Guo, Y. Li, D. Zhu, Architecture of Graphdiyne Nanoscale Films, Chem. Commun. 46 (2010) 3256-3258.

[13] J. Zhong, J. Wang, J.-G. Zhou, B.-H. Mao, C.-H. Liu, H.-B. Liu, et al., Electronic Structure of Graphdiyne Probed by X-ray Absorption Spectroscopy and Scanning Transmission X-ray Microscopy, J. Phys. Chem. C 117 (2013) 5931-5936.

[14] J.Y. Zhou, X. Gao, R. Liu, Z.Q. Xie, J. Yang, S.Q. Zhang, et al., Synthesis of Graphdiyne Nanowalls Using Acetylenic Coupling Reaction, J. Amer. Chem. Soc. 137 (2015) 7596-7599.

[15] K. Tahara, Y. Yamamoto, D.E. Gross, H. Kozuma, Y. Arikuma, K. Ohta, et al., Syntheses and Properties of Graphyne Fragments: Trigonally Expanded Dehydrobenzo[12]annulenes, Chem. Eur. J. 19 (2013) 11251-11260.

[16] J.L. Kou, X.Y. Zhou, H.J. Lu, F.M. Wu, J.T. Fan, Graphyne as the membrane for water desalination, Nanoscale 6 (2014) 1865-1870.

[17] H.J. Hwang, J. Koo, M. Park, N. Park, Y. Kwon, H. Lee, Multilayer Graphynes for Lithium Ion Battery Anode, J. Phys. Chem. C 117 (2013) 6919-6923-

[18] P. Wu, P. Du, H. Zhang, C.X. Cai, Graphyne As a Promising Metal-Free Electrocatalyst for Oxygen Reduction Reactions in Acidic Fuel Cells: A DFT Study, J. Phys. Chem. C 116 (2012) 20472-20479.

[19] A. Ruiz Puigdollers, P. Gamallo, DFT study of the role of N- and B-doping on structural, elastic and electronic properties of α-, β- and γ-graphyne, Carbon 114 (2017) 114, 301-310.

[20] R.J. Liu, H.B. Liu, Y.L. Li, Y.P. Yi, X.K. Shang, S.S. Zhang, et al., Nitrogen-doped graphdiyne as a metal-free catalyst for high-performance oxygen reduction reactions, Nanoscale 6 (2014) 11336-11343.

[21] H.J. Hwang, Y. Kwon, H. Lee, Thermodynamically Stable Calcium-Decorated Graphyne as a Hydrogen Storage Medium, J. Phys. Chem. C 116 (2012) 20220-20224.

[22] U. Sakar, B. Bhattacharya, N. Seriani, First Principle Study of Sodium Decorated Graphyne, Chem. Phys. 461 (2015) 74-80.

[23] B. Jang, J. Koo, M. Park, H. Lee, J. Nam, Y. Kwon, et al., Graphdiyne as a High-Capacity Lithium Ion Battery Anode Material, Appl. Phys. Lett. 103 (2013) 263904.

[24] S.-H. Lee, S.-H. Jhi, A first-principles study of alkali-metal-decorated graphyne as oxygen-tolerant hydrogen storage media, Carbon 81 (2015) 418-425.

[25] B. Xu, X.L. Lei, G. Liu, M.S. Wu, C.Y. Ouyang, Li-decorated graphyne as high-capacity hydrogen storage media: First-principles plane wave calculations, Int. J. Hydrogen Energy 39 (2014) 17104-17111.

[26] M. Manadé, F. Viñes, F. Illas, Transition metal adatoms on graphene: A systematic density functional study, Carbon 95 (2015) 525-534.

[27] X. Qian, Z. Ning, Y. Li, H. Liu, C. Ouyang, Q. Chen, et al. Construction of graphdiyne nanowires with high-conductivity and mobility, Dalton Trans. 41 (2012) 730-733.

[28] Z.-Z. Lin, Q. Wei, X. Zhu, Modulating the electronic properties of graphdiyne nanoribbons, Carbon 66 (2014) 504-510.

[29] J.P. Perdew, K. Burke, M. Ernzerhof, Generalized Gradient Approximation Made Simple, Phys. Rev. Lett. 77 (1996) 3865-3868.

[30] S. Alaei, S. Jalili, S. Erkoc, Study of the Influence of Transition Metal Atoms on Electronic and Magnetic Properties of Graphyne Nanotubes Using Density Functional Theory, Fuller. Nanotub. Car. N. 23 (2014) 494-499.

[31] T. Kawase, Y. Seirai, H.R. Darabi, M. Oda, Y. Sarakai, K. Tashiro, All-Hydrocarbon Inclusion Complexes of Carbon Nanorings: Cyclic [6]- and [8]Paraphenyleneacetylenes, Angew. Chem. Int. Ed. 42 (2003) 1621-1624.

[32] F. Bonaccorso, L. Colombo, G. Yu, M. Stoller, V. Tozzini, A.C. Ferrari, et al., Graphene, related two-dimensional crystals, and hybrid systems for energy conversion and storage, Science 347 (2015) 1246501.

[33] Z.-Z. Lin, Graphdiyne-supported single-atom Sc and Ti catalysts for high-efficient CO oxidation, Carbon 108 (2016) 343-350.

[34] E. Azizi, Z.A. Tehrani, Z. Jamshidi, Interactions of small gold clusters, Aun (n = 1-3), with graphyne: Theoretical investigation, J. Mol. Graph. Model. 54 (2014) 80-89.

[35] S. Grimme, Semiempirical GGA-type density functional constructed with a long-range dispersion correction, J. Comput. Chem. 27 (2006) 1787-1799.

[36] A. Ruiz Puigdollers, G. Alonso, P. Gamallo, First-principles study of structural, elastic and electronic properties of α-, β- and γ-graphyne, Carbon 2016, 96, 879-887.

[37] G. Kresse, J. Furthmüller, Efficient iterative schemes for ab initio total-energy calculations using a plane-wave basis set, Phys. Rev. B 54 (1996) 11169-11186.

[38] P.E. Blöchl, Projector augmented-wave method, Phys. Rev. B 50 (1994) 17953-17979.

[39] B. Kang, H. Liu, J.Y. Lee, Oxygen adsorption on single layer graphyne: a DFT study, Phys. Chem. Chem. Phys. 16 (2014) 974-980.

[40] P. Janthon, S.M. Kozlov, F. Viñes, J. Limtrakul, F. Illas, Establishing the accuracy of broadly used density functionals in describing bulk properties of transition metals, J. Chem. Theory Comput. 9 (2013) 1631-1640.

[41] P. Janthon, S.J. Luo, S.M. Kozlov, F. Viñes, J. Limtrakul, D.G. Truhlar, et al., Bulk Properties of transition metals: A challenge for the design of universal density functionals, J. Chem. Theory Comput. 10 (2014) 3832-3839.

[42] H.J. Monkhorst, J.D. Pack, Special points for Brillouin-zone integrations, Phys. Rev. B 13 (1976) 5188-5192.

[43] P. Janthon, F. Viñes, S.M. Kozlov, J. Limtrakul, F. Illas, Theoretical assessment of graphene-metal contacts, J. Chem. Phys. 183 (2013) 244701.

[44] H. Muñoz-Galán, F. Viñes, J. Gebhardt, A. Görling, F. Illas, The contact of graphene with Ni(111) surface: description by modern dispersive forces approaches, Theo. Chem. Acc. 135 (2016) 165.

[45] M. Amft, S. Lebègue, O. Eriksson, N.V. Skorodumova, Adsorption of Cu, Ag, and Au atoms on graphene including van der Waals interactions, J. Phys.: Condens. Matter 23 (2011) 395001

[46] S. Grimme, J. Antony, S. Ehrlich, S. Krieg, A consistent and accurate ab initio parametrization of density functional dispersion correction (DFT-D) for the 94 elements H-Pu, J. Chem. Phys. 132 (2010) 154104.

[47] A. Tkatchenko, R.A. Di Stasio, R. Car, M. Scheffler, Accurate and efficient method for many-body van der waals interactions, Phys. Rev. Lett. 108 (2012) 236402.

[48] R.F. Bader, Atoms in Molecules: A Quantum Theory, Oxford Science, Oxford, U.K., 1990.

[49] F. Viñes, C. Loschen, F. Illas, K.M. Neyman, Edge sites as a gate for subsurface carbon in palladium nanoparticles, J. Catal. 266 (2009) 59-63.